Polymer Degradation and Stability 237 (2025) 111321

Contents lists available at ScienceDirect

Polymer Degradation and Stability

journal homepage: www.journals.elsevier.com/polymer-degradation-and-stability

Novel one-pot recovery and *in-situ* crystallization of polyhydroxybutyrate and hydroxyapatite/tricalcium phosphate biocomposite microparticles with comparative life cycle assessment

Anuchan Panaksri [a,1], Pasin Kuncharin [a,1], Purin Neerawong [a,1], Taranuch Panthong [a], Thanadol Thanakornkriengkrai [a], Sani Boonyagul [a], Woradej Pichaiaukrit [b], Sutee Wangtueai [c,d], Nuankanya Sathirapongsasuti [e,f], Kittisak Jantanasakulwong [d,g], Pornchai Rachtanapun [d,g], Patnarin Worajittiphon [h], Phavit Wongsirichot [i], Nuttapol Tanadchangsaeng [a,*]

[a] College of Biomedical Engineering, Rangsit University, Pathum Thani 12000, Thailand
[b] College of Dental Medicine, Rangsit University, Pathum Thani 12000, Thailand
[c] School of Agro-Industry, Faculty of Agro-Industry, Chiang Mai University, Chiang Mai 50200, Thailand
[d] Center of Excellence in Agro Bio-Circular-Green Industry (Agro BCG), Chiang Mai University, Chiang Mai 50200, Thailand
[e] Chakri Naruebodindra Medical Institute, Faculty of Medicine Ramathibodi Hospital, Mahidol University, Samut Prakan 10540, Thailand
[f] Program in Translational Medicine, Faculty of Medicine Ramathibodi Hospital, Mahidol University, Bangkok 10400, Thailand
[g] Packaging Technology Division, School of Agro-Industry, Faculty of Agro-Industry, Chiang Mai University, Chiang Mai 50200, Thailand
[h] Department of Chemistry, Faculty of Science, Chiang Mai University, Chiang Mai 50200, Thailand
[i] Department of Chemical Engineering, The University of Manchester, Manchester, M13 9PL, United Kingdom

ARTICLE INFO

Keywords:
Polyhydroxyalkanoates
In-situ crystallization
Cupriavidus necator
Biopolymer recovery
Biocomposite
Hydroxyapatite
Tricalcium phosphate
Life cycle assessment

ABSTRACT

Formation of polyhydroxybutyrate (PHB) biopolymer composites with bioceramics such as hydroxyapatite (HA) and tricalcium phosphate (TCP) is essential in achieving mechanical properties needed for novel bone tissue engineering using PHB. However, composite microparticle synthesis typically requires multiple steps, including 1) PHB recovery and purification, 2) dispersion of HA and TCP particles in the melt or solvent-dissolved polymer liquid, and 3) micro-droplet drying. In this study, PHB/HA/TCP composite microparticles were successfully produced by one-pot biosynthesis. This was achieved during acid-based PHB recovery by utilizing the crystallization of native-amorphous granule PHB within *Cupriavidus necator*. In-situ PHB crystallization was successfully monitored by real-time attenuated total reflection-Fourier transform infrared (ATR-FTIR). Additionally, the in-situ crystallization behavior was elucidated by scanning electron microscopy (SEM) and transmission electron microscopy (TEM). The most suitable conditions for synthesis of the PHB/HA/TCP composite were pH 2, and 20 min of reaction time, which capitalizes on the amorphous nature of the in-situ PHB during recovery. The HA and TCP did not function as nucleating agents, thereby not impacting accumulation and homogeneity. This allows HA/TCP bioceramics to be inserted into the polymer during the PHB recovery period, and after the crystallization step is completed, the composite microparticles could facilely form. The crystallization mechanism was found to be sporadic, and the morphology was a disc with two dimensions. Additionally, the life cycle assessment (LCA) revealed that the one-pot method reduced global warming potential (GWP) emissions by 50% and non-renewable energy use (NREU) by a comparable margin, compared to the conventional multi-step method for HA/TCP (20:80) production. These findings emphasize the environmental advantages of the one-pot approach alongside its cost and process efficiency. The demonstrated one-pot synthesis method would allow for more streamlined and cost-effective production of PHB/HA/TCP biocomposites. The materials produced and insights gained will be beneficial for future development of biopolymer composite processing and biomedical applications.

* Corresponding author.
E-mail address: nuttapol.t@rsu.ac.th (N. Tanadchangsaeng).
[1] These authors equally contributed to this research

https://doi.org/10.1016/j.polymdegradstab.2025.111321
Received 14 January 2025; Received in revised form 4 March 2025; Accepted 9 March 2025
Available online 10 March 2025

1. Introduction

Polyhydroxybutyrate (PHB) is a polyester in the polyhydroxyalkanoates (PHAs) family [1], which is a natural polymer synthesized intracellularly by bacteria such as *Bacillus megaterium* and *Cupriavidus necator* [2]. Due to its biodegradable nature, non-toxicity, absence of carcinogenicity, and biocompatibility [3], PHB is an ideal candidate for novel biomaterials in biomedical applications such as tissue engineering [4]. Specifically, in bone tissue engineering, PHB facilitates new bone regeneration by providing essential mechanical support [5]. To enhance the mechanical properties requisite for bone substitution [6], PHB is often blended or composited with calcium phosphate ceramics such as hydroxyapatite (HA) and β-tricalcium phosphate (β-TCP) [7], to mimic the structural and functional complexity of natural bone tissue [8].

HA is the predominant form of calcium phosphate, the primary inorganic bone phase. HA is an extremely useful material for various biomedical applications due to its biocompatibility, bioactivity, osteoconductive, osteoinductive, and osteointegration properties [9]. Leading to various applications of HA, such as bone implants and prostheses in the orthopedic field [10], drug delivery systems, coating of implants, and bone grafts and scaffolds for tissue engineering [11]. However, HA is hardly resorbed, so it is maintained in the augmentation site and reduces new bone formation. This may not be suitable for certain types of treatments, such as those requiring rapid new bone formation. Another bone phase material, TCP has higher degradability than HA, cell-mediated resorption [12], osteoconduction, and osteoinduction and is readily replaced by new bone. It is widely employed in dental and orthopedic applications for regeneration [13]. The mixture between HA and TCP granules can work together synergistically, as demonstrated by Sanda et al. (2015) [14], concluded that the mixed material could maintain the volume of the grafted site, and TCP showed degradation, which demonstrates their potential as bone replacement. Afterward, the mixed material has been utilized in several studies [15] for bone regeneration [16].

Composite microparticle synthesis typically requires multiple steps, including 1) PHB recovery and purification, 2) dispersion of HA and TCP particles in the melt or solvent-dissolved polymer liquid, and 3) subsequent micro-droplet drying processes. In-situ crystallization for the production of PHB/HA/TCP could potentially lead to a more streamlined composite synthesis scheme, which could potentially reduce the time and costs of future production of the biomaterial. However, to date, the incorporation of in-situ crystallization for PHB/HA/TCP composite synthesis has not yet been explored. In-situ crystallization could take advantage of the phase transition of PHB during recovery, to integrate other materials within a matrix, such as HA and TCP, thus forming a composite. This phase transition can be induced because PHB accumulates in an amorphous form within the cells of the producer microorganisms [17], and acidic PHB extraction method can be used to cause a phase transition from the amorphous state to a well-organized polymer chain arrangement, eventually crystallizing into a solid form [18].

Although there are studies on composites of HA or TCP with PHA, most of these involve using structured PHA and mixing it with micrometric particles of ceramics. However, in the microscale, there is limited research where PHB particles serve as a medium to connect with HA and TCP particles. Some studies have explored this using the sol-gel method [19], but with different types of polymers, due to thermal degradation limitations that prevent the use of high temperatures typically used in HA and TCP composites, such as hydrothermal hot-pressing (HHP) [20].

For the first time, PHB/HA/TCP composite synthesis via a one-pot in-situ crystallization and polymer recovery scheme will be investigated. Important parameters, behavior and trends associated with the one-pot composite production will be elucidated. This includes investigation into interaction between the PHB with HA and β-TCP during phase transition and whether this interaction could lead to enhanced material properties. Additionally, characterization of PHB/HA/TCP composite microparticles with respect to the physical and chemical properties, including morphology, homogeneity, particle size, and crystallinity was conducted, to indicate their suitability for novel biomedical applications, in particular for dental bone restoration. In addition to material performance, the environmental implications of this novel synthesis method were also considered. A life cycle assessment (LCA) was conducted to evaluate the environmental impacts of the one-pot in-situ crystallization approach compared to conventional multi-step production methods. The analysis focused on key environmental indicators, such as global warming potential (GWP) and non-renewable energy use (NREU), providing a broader perspective on the potential sustainability of this innovative approach. The novel composite synthesis method developed and the insights provided will be useful for future development of PHA downstream processing, biomedical PHA composites synthesis and biopolymer valorization in general.

2. Materials and methods

2.1. Materials

Cupriavidus necator ATCC 17,699 was purchased from American Type Culture Collection (VA, USA). Glycerol (99%) and sodium hypochlorite (NaHOCl) were purchased from Hong Huat Company Limited (Thailand). Dipotassium phosphate (K_2HPO_4), disodium phosphate (Na_2HPO_4), and ammonium sulfate $(NH_4)_2SO_4$) were purchased from Ajax Finechem (New Zealand). Nutrient broth, sulfuric acid (H_2SO_4), sodium hydroxide (NaOH), hydroxyapatite ($Ca_{10}(PO_4)_6(OH)_2$), magnesium sulfate ($MgSO_4$), and tricalcium phosphate ($Ca_3(PO_4)_2$) were purchased from Sigma-Aldrich (St. Louis, MO, USA). Chloroform was purchased from RCI Labscan (Thailand).

2.2. Bacterial cultivation for polyhydroxybutyrate synthesis

PHB production using *C. necator* was conducted in a 250 mL shake flask for 24–48 h, using conditions based on a previous study [21]. The bacterial cultivation used 75% glycerol as a carbon source, and the mineral salts (MS) medium consisted of 7.34 g/L K_2HPO_4, 1.20g/L Na_2HPO_4, and 2 g/L $(NH_4)_2SO_4$. The procedure is as follows: (1) activate 2 mL of *C. necator* in 5 mL of nutrient broth in a 10 mL in vitro setup and incubate for 24 h at 30 °C and 180 rpm, (2) after 24 h, transfer the broth into 50 mL flasks, then added carbon source of 20 g/L and $MgSO_4$ 0.5 g/L and incubate for an additional 48 h at 30 °C and 180 rpm, and 3) after the strain has been incubated for 48 h, add it to 200 mL of MS, a carbon source of 20 g/L, and $MgSO_4$ of 0.5 g/L in a 250 mL flask. Then, incubate for another 48 h at 30 °C and 180 rpm. PHB content of the final broth was assessed by taking a 2 mL aliquot, while the remaining broth was used for biocomposite synthesis. The *C. necator* cells were harvested by centrifugation at 6000 rpm for 20 minutes, resulting in a wet cell pellet. The wet cell pellet was then treated with 20% H_2SO_4, adjusting the pH to 2, to preserve the biomass before proceeding to the extraction and composite synthesis process.

2.3. Extraction of PHB and composite synthesis with hydroxyapatite and tricalcium phosphate

An acid-base extraction method was chosen to separate the PHB from the cell biomass based on the previous study, which demonstrates it as an efficient and ecologically sustainable technique for PHA extraction and purification [22]. The bacterial cell wall was disintegrated by adding 20% (v/v) H_2SO_4 to the broth and adjusting the pH to 2. In-situ composite synthesis was subsequently conducted by adding HA and TCP to the solution at different ratios between PHB and the bioceramics (Table 1). The proportion of HA to TCP was maintained at 20% wt. HA and 80% wt. TCP, which is the proportions for use as a bone substitute indicated in the literature [23]. The solution was stirred at 150 rpm for 40 min at room temperature. Afterward, the solution's pH was adjusted

Table 1
Ratio of HA and TCP that incorporated with PHB.

Designation	PHB (% wt.)	HA (% wt.)	TCP (% wt.)
PH0T0	100	0	0
PH1T4	95	1	4
PH2T8	90	2	8
PH4T16	80	4	16
PH8T32	60	8	32

to 13 using 5 M NaOH and left for 30 min to solidify the PHB at room temperature. A 6% (w/v) NaClO solution was then added to the mixed solution at a 1:1 vol ratio. The mixture was stirred at 150 rpm for 1 h at room temperature. The PHB/HA/TCP composite microparticles were separated from the solution using centrifugation at 6000 rpm for 30 min. The centrifuged micro-particle precipitate was washed with an equal volume of deionized water (DI), resulting in a white-colored solution. The suspended PHB/HA/TCP microparticles in the DI were stirred at room temperature for 1 h and then centrifuged at 6000 rpm for 30 min. The micro-particle precipitate obtained from the centrifugation was dried using a hot air oven at 60 °C for 24 h, producing the PHB/HA/TCP micro-particle samples for further characterization.

2.4. Homogeneity and particle size analysis

The homogeneity of the PHB/HA/TCP microparticles was measured using samples of the microparticles suspended in DI water via zeta potential measurements, which evaluate the stability of suspended particles in a liquid. This method determines the homogeneity of the surrounding composite particles and is often coupled with particle size analysis. The zeta potential measurement was conducted using a Particle Size Analyzer with a sample volume of 2 mL, placed in a flow cell attached to an analyzer. Zeta potential readings were processed using the Delsa^{TM} Nano software version 2.21 (Beckman Coulter, USA). The program was set at 25 °C for 25 s, and the dilution solvent was DI water.

Particle size analysis was performed using laser diffraction and polarization intensity differential scattering (PIDS). A 2 mL of PHB/HA/TCP solution was placed in a particle size measurement cell installed in the particle size analyzer. Particle measurement of the sample was carried out using the Delsa Nano C software, with the same temperature, time, and dilution settings as the zeta potential measurement.

2.5. Characterization of biocomposite crystallinity

Attenuated total reflection-Fourier transform infrared (ATR-FTIR) was used to characterize the PHB/HA/TCP composite microparticles, comparing with the X_c (X-ray crystallinity) obtained from XRD (X-ray diffraction). The relativity technique utilizes X-ray to analyze the crystal structure of the compounds in the specimen, allowing the determination of crystallinity by measuring the absorbance of the infrared spectra of composite microparticles PHB/HA/TCP with FTIR spectrometer. Suspended samples of PHB/HA/TCP composite microparticles (5 μL) were scanned in the ATR window at room temperature. A total of 32 scans of absorbance spectra were measured every 1 to 2 min for a total of 6 min to obtain a PHB/HA/TCP composite microparticle spectral absorbance curve. The infrared absorption intensity of each wavenumber was calculated, as shown in Eq. 1, to plot a comparative curve and find the most prominent infrared absorption intensity [24].

$$A_{PHB\ w} = A_{total} - A_{background} \quad (1)$$

where $A_{PHA\ w}$ is the infrared absorption intensity of PHB at that wavenumber, A_{total} is the infrared absorption intensity at peak, and $A_{background}$ is the infrared absorbance intensity at a ground point.

Next, the Instantaneous absorption index was determined by dividing the most prominent infrared absorption intensity (evident) by the reference infrared absorption intensity (reference), which represents constant absorption of infrared light as shown in Eq. 2.

$$AI_I = \frac{A_{Evident}}{A_{Reference}} \quad (2)$$

where AI_I is the instantaneous infrared absorption index, $A_{Evident}$ is PHB's most prominent infrared absorption intensity, and $A_{Reference}$ is the reference infrared absorption intensity of PHB.

Then, the absorbance infrared spectra values of six standard PHAs were compared with Xc values from XRD (Tanadchangsaeng and Yu, 2013) to produce a calibration curve, which was used to determine the crystallinity of the previous AI_I equation [25].

The six PHA samples can be categorized as follows: PHB synthesized using glycerol as a substrate. Sample A, the original poly(3-hydroxybutyrate-co-3-hydroxyvalerate-co-4-hydroxyvalerate) (PHBVV) copolymer, was synthesized using glycerol and levulinic acid as substrates in a previous study, and in this work, it was referenced solely for its absorbance and crystallinity values [25]. Fractions A1, A2, and A3, which are fractionated PHBVV copolymers from Sample A, were obtained through a meticulous fractional extraction process using chloroform. Lastly, MCL-PHA (medium-chain-length polyhydroxyalkanoate), a type of PHA, was produced by using sodium octanoate as the substrate. Each of these samples represents a unique method of PHA production, providing a diverse range of materials for study. These standard PHA samples were used as reference materials for crystallinity analysis and calibration curve construction. Eq. 3 can then be used to form the calibration curve (crystallization curve).

$$X_i = mAI_i + b \quad (3)$$

where Xi is instantaneous crystallinity, AIi is instantaneous infrared absorption index, m is slope, and b is intercept of the calibration lines.

The data obtained from the crystallization curve can be used with the Avrami equation (Eq. 4) in its logarithmic form (Eq. 5). The Avrami exponent (n) and growth rate parameter (k) are employed to elucidate the crystallization behavior of polymer during spherulite formation. This allows the constants n and k to be determined, indicating the morphology and mechanism of crystallization. Meanwhile, the crystallization half-time can be found using Eq. 6.

$$1 - X_t = exp(-kt^n) \quad (4)$$

$$\log[-In(1-x_t)] = log\ k + log\ t \quad (5)$$

where k is the crystallization rate constant, t is the crystallization time (min), n is the Avrami constant, and X_t is the crystalline volume fraction at a constant time.

$$t1/2 = \left(\frac{In2}{k}\right)^{1/n} \quad (6)$$

where $t1/2$ is the half-time of crystallization, k is the crystallization rate constant, and n is the Avrami constant (depending on dimension).

2.6. Morphology analysis

A scanning electron microscope (SEM) was used to capture images at a resolution of 256 × 192 pixels. SEM samples were prepared as follows. The PHB/HA/TCP composite microparticles underwent heating at 60 °C for 24 h, affixed to aluminum using carbon double-sided electrical tape, and coated with gold. Transmission electron microscopy (TEM) images were observed at 100 kV and photographed with a frame-transfer Charge Coupled Device (CCD) camera. TEM was conducted to visualize the intracellular localization of PHB/HA/TCP. At room temperature, cells were fixed with 2.5 % glutaraldehyde in 0.1 M phosphate-buffered saline (PBS) at pH 7.4 for 1–2 h. Subsequently, they were left for 2 h, centrifuged at 6000 rpm for 30 min, and the fixative was discarded. The cells were then washed three times in 0.1 M PBS for 15–20 min each

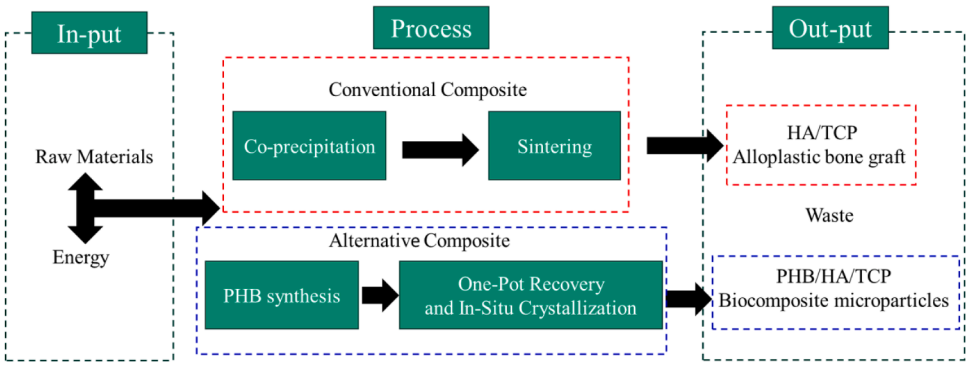

Fig. 1. Assessment boundaries of conventional and one-pot processes for PHB/HA/TCP production.

time. After centrifugation, the cells' buffer was removed. Next, post-fixation involved osmium tetroxide with 0.1 M PBS in the hood for 2 h. The cells were then centrifuged, the translucent part removed and washed in 0.1 M PBS and DI for one change of 15–20 min each. After centrifugation, the translucent part was removed, and the cells were mixed with 2% agar, melted, and left at 45–50 °C until solidified. The agar was then cut into small square pieces of not more than 0.5 cubic millimeters and dehydrated with 35%, 70%, and 95% ethanol for 15–20 min each. Three more cycles of dehydration with absolute ethanol, each lasting 15–20 min, were performed. Following absolute ethanol dehydration, soaking in propylene oxide occurred three times for 15–20 min each. Cell infiltration was done with Spurr's resin, mixed with propylene oxide at ratios 1:3, 1:1, and 3:1 ratio for 3 h overnight, was followed by further infiltration with Spurr's resin for 3 h overnight, and repeated 3 times. The sample was then incubated in an oven at 70 °C for 8 h, cut with an ultramicrotome to section thickness of 80 nm, placed on a copper grid, and stained with uranyl acetate and lead citrate to enhance contrast. The sample was finally observed using TEM operating at 800–1000 kV.

2.7. Cell cytotoxicity

According to ISO 10,993–5, the MTT test was used to determine how cytotoxic the substance was. A 96-well plate was seeded with 100 μL of MC3T3-E1 cells at 1×10^4 cells/well density. Then, 100 μL of the sterilized material was placed and incubated for 24, 48, and 72 h at 37 °C in a humidified 5% CO_2 atmosphere. A 50 μL MTT reagent (1 mg/mL DMEM without phenol red) was added after each culture phase, and it was then incubated for 4 hours at 37 °C. The solution in each well was drained after the incubation period, and 100 μL DMSO was added to dissolve the precipitated formazan crystals. In order to assess light absorption at a wavelength of 570 nm, the well plate was placed in a microplate reader (EPOCH, BioTek Instruments, Winooski, VT, USA). The percentage of cell viability was calculated to estimate cell cytotoxicity using the equation below:

Cell viability (%) = (absorbance of experimental group / absorbance of control group) x 100

The control group consisted of cells cultured in DMEM without any material, while the experimental group consisted of cells cultured in DMEM with the sterilized material being tested. A material is considered cytotoxic if the cell viability is less than 70%.

Table 2
Data inputs used for assessing compositing method.

Material/Energy	Unit/Functional (0.15 g)*	Conventional process	One-pot process
Substance			
Calcium chloride ($CaCl_2$)	g	0.162	-
Sodium phosphate ($Na_3PO_4{\cdot}12H_2O$)	g	0.363	-
Deionized water	mL	90	6
Sulfuric acid (H_2SO_4) 20%	mL	0.075	0.12
Sodium hydroxide (NaOH)	g	0.03	0.0072
Mineral salts (MS medium)	mL	-	32.26
Cupriavidus necator (inoculum)	mL	-	0.65
Glycerol	g	-	0.65
Hydroxyapatite (HA)	g	-	0.006
Tricalcium phosphate (TCP)	g	-	0.024
Sodium Hypochlorite (NaOCl) (6%, w/v)	mL	-	0.12
Energy			
Electricity for stirring	kWh	0.2	0.2
Electricity for heating/ stirring	kWh	0.5	0.4
Electricity for sintering (900 °C)	kWh	2.5	-
Electricity for shaking (30 °C, 180 rpm)	kWh	-	0.6
Electricity for centrifugation	kWh	-	0.4

* The amount of substance used per functional unit of 0.15 g, corresponding to the material required for implantation in a 15 × 10 mm^2 wound.

2.8. Life cycle assessment (LCA)

The life cycle assessment (LCA) was conducted in accordance with ISO 14,040 and 14,044 standards, adopting a gate-to-gate assessment approach. The objective of this study was to evaluate the environmental impacts associated with the production of PHB/HA/TCP composite microparticles as a material for bone regeneration in dental sockets. This was compared with a conventional alloplastic bone graft product available in the market. The functional unit was defined as the amount of material required for implantation in a 15 × 10 mm^2 wound, which corresponds to 0.15 g of material. The production processes and assessment boundaries for both materials are illustrated in Fig. 1, and the inventory data, including chemicals and energy used in the

Table 3
Particle size and zeta potential of PHB/HA/TCP composite microparticle (n=3).

Sample code	Particle size (μm)	Zeta potential (mV)
PH0T0	0.9 ± 0.08	-47.24 ± 1.79
PH1T4	111.31 ± 13.42	-16.60 ± 1.69
PH2T8	220.70 ± 31.92	-21.80 ± 1.57
PH4T16	332.96 ± 27.18	-35.65 ± 2.48
PH8T32	386.02 ± 36.83	-31.40 ± 1.63
HA20/TCP80	ND*	-1.61

* ND is not determined.

processes, are presented in Table 2. The data were analyzed to assess environmental impacts using SimaPro 9.6 software (PRé Sustainability, Amersfoort, Netherlands) and the Ecoinvent database version 3.9.1. The assessment employed the IMPACT World+ Midpoint methodology, focusing on two impact categories: global warming potential (GWP) and non-renewable energy use (NREU).

3. Results and discussion

3.1. Polyhydroxybutyrate production

The cell density of the cultured C. necator in a 50 mL volume was determined to be 38.98 g/L (dry cell weight). The extractable PHB content was 3.72 g/L, corresponding to an extraction recovery of 9.6% relative to the total dry cell weight. The extracted PHB exhibited a molecular weight (Mw) of 550 kDa and a purity of 95%, confirming its high quality for further biocomposite synthesis. The HA and TCP bioceramic components were added in proportion to the 3.72 g/L PHB concentration to produce the designated composite formulations, as shown in Table 1.

3.2. Homogeneity and particle size of PHB/HA/TCP composite

The zeta potential and size measurements of the PHB/HA/TCP microparticles are presented in Table 3. The zeta potential indicates the stability of the particles suspended in the liquid [26]. A sample with a high stability value suggests that its particles can distribute well within the liquid [27]. Samples with a zeta potential ranging from ± 30 to ± 60 are considered stable [28]. Table 3 indicates that the pure PHB has the zeta potential value farthest from zero. The zeta potential value increases when bioceramics are incorporated at low quantities. Therefore, as the composite begins to include small amounts of HA and TCP, the stability of the sample decreases. The most stable microparticle PHB/HA/TCP sample consists of 80% PHB and 20% bioceramics, divided into 4% HA and 16% TCP (PH4T16), with a zeta potential value of -35.65 mV. Compositing the bioceramics with PHB improves their overall zeta potential and suspension stability, as pure HA20/TCP80 only has a zeta potential of -1.61 mV. The low stability of HA20/TCP80 could lead to unwanted settling or agglomeration during processing. This negatively affects the efficiency of dental bone restoration due to the uneven distribution of active substances. Thus, PHA compositing should lead to improved processing and bone restoration. Comparing the zeta potentials reveals that PH4T16, which is stable when suspended in liquid, might be applied in dental bone restoration treatments. Its good dispersion might enhance cell contact, potentially leading to more effective regeneration [29].

From Table 3, it can be seen that the size of the microparticles increases with the amount of HA and TCP. The particle size of PHB, which has not been compounded with bioceramics, is approximately 0.9 μm. In contrast, the size of the PHB/HA/TCP microparticles ranges between 100–400 μm, falling within the same criteria as materials used in dental transplantation with a functional range of 200–1000 μm. This is a range where the particle size can enhance the formation of dental bone well [30]. The size of the composite particles is larger than that of the non-composite PHB particles, which are only 0.9 μm in size. The difference between these particles helps confirm that the bioceramic particles have agglomerated with the PHB particles. Since the incorporation of HA and TCP with PHB occurs with native PHB, the integration of HA and TCP with PHB might take place in conditions where the PHB has not

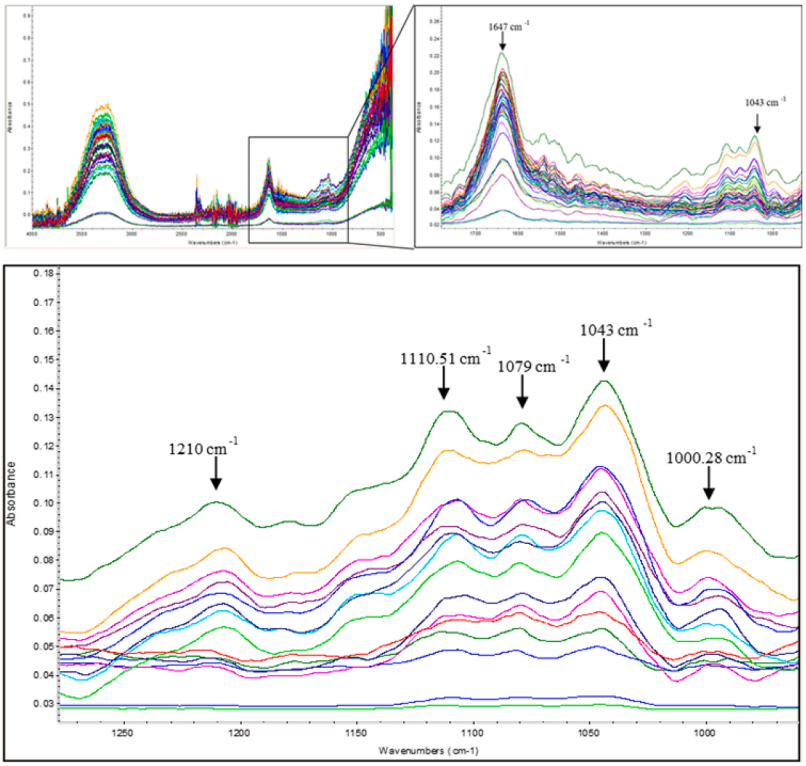

Fig. 2. The absorbance of composite microparticles of PHB/HA/TCP measured by FTIR method.

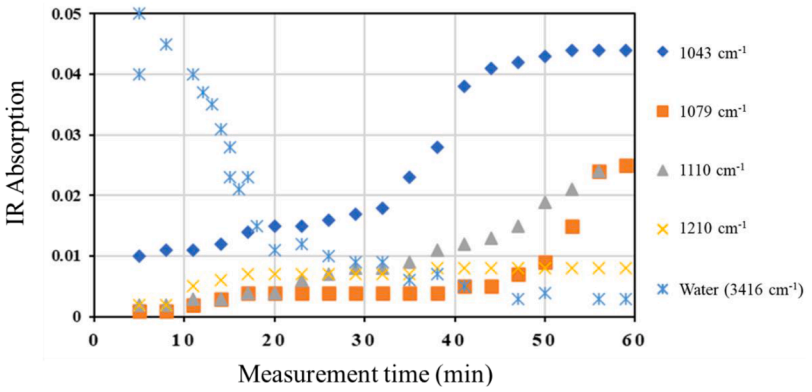

Fig. 3. The absorbance of composite microparticles of PHB/HA/TCP compared with time.

yet been able to form a solid mass. This might cause the particle size to increase when both types of bioceramics are added to the PHB structure. It appears that PHB particles serve as nucleation sites for the accumulation of additional particles during the crystallization process, which leads to an increase in the size of the material particles. This increased sized, importantly allows for the composite particles to be used for the targeted dental transplantation.

The results from both measurements suggest that the biocomposite samples are homogeneous, as evidenced by the trend of increased particle size with increasing bioceramic ratio and the even distribution of particles indicated by the zeta potential values. The increase in particle size suggests that HA and TCP are well-integrated into the PHB matrix rather than forming irregular clusters, while the zeta potential values indicate that electrostatic stabilization prevents uncontrolled particle aggregation. This stability ensures that particles remain dispersed rather than forming large agglomerates, which could otherwise lead to inconsistencies in material properties. Thus, indicating that there are no varied particle sizes or particle agglomerations in the liquid. The homogeneity of these biocomposite materials is crucial for their subsequent processing and applications. A homogeneous material ensures consistent properties throughout, which is vital for achieving reliable performance in applications [31]. For instance, in scenarios where the material is in constant contact with a liquid medium, such as in certain dental and orthopedic applications, the homogeneity of the material can influence its interaction with the liquid medium and its overall performance. Therefore, the observed homogeneity of the PHB and HA/TCP biocomposite materials is a promising indicator for their potential use in such applications. For orthopedic or dental uses for osteogenesis, the homogeneity of the PHB and HA/TCP biocomposite materials can play a significant role. In dental applications, such as the fabrication of dental implants or scaffolds for bone regeneration, the homogeneity of the material can ensure consistent degradation rates, which is crucial for the gradual replacement of the implant with natural tissue. Similarly, in orthopedic applications, such as the repair of bone defects or the replacement of joint surfaces, the homogeneity of the material can influence its mechanical properties, such as strength and toughness, which are critical for the long-term success of the implant [32]. Therefore, the observed homogeneity of these biocomposite materials not only indicates their potential use in these applications but also suggests their potential to enhance the performance and reliability of dental and orthopedic implants [33].

3.3. *Crystallization test with ATR - FTIR spectroscopy*

Fig. 2 displays the absorbance or the light spectrum of the PH4T16 composite microparticles using FTIR. Following the addition of HA and TCP with 20% acid solution (H_2SO_4) until pH 2, it was observed that the spectrum at min 0 (bottom line) still corresponded to an amorphous polymer. By the 30th min (green line) the spectrum characteristics completely crystallized. After 60 min (top line), all five peaks were detected after completing crystallization. The FTIR measurement results demonstrate the tracking of the crystallization process of the PHB composite particles. This is observed from the increasing absorbance values from the baseline at each time interval until complete crystallization. The increasing absorbance over time may reflect the phase change of PHB from the amorphous state to the crystalline state, which can be reflected in changes to the molecular structure of PHB.

Real-time measurement of the crystallinity of materials, by tracking the phase change behavior of materials, is very important in explaining how HA and TCP particles play a role during the time when PHB serves

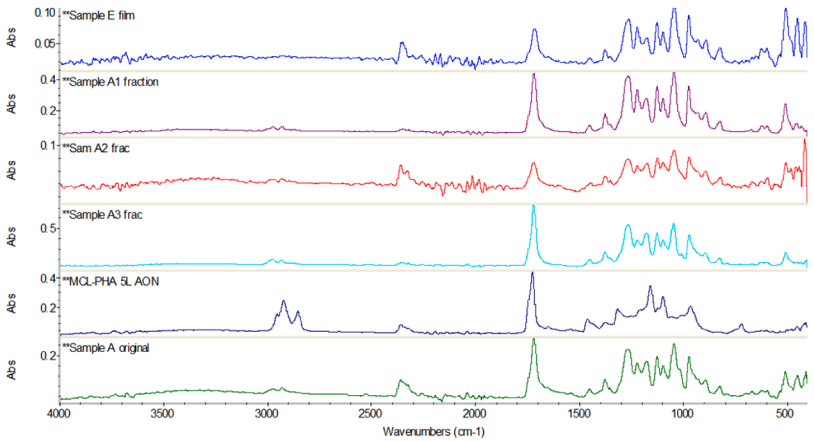

Fig. 4. The infrared spectral absorbance curves of all six standard PHAs.

Table 4
Infrared spectral absorbance of six standard PHA polymers compared to the X_c values.

Sample	Absorbance of infrared spectra at wavenumber of 1043 cm^{-1}	X_c (XRD)	Ref.	Molecular weight (M_w) (kDa)
PHBVV (Sample A)	0.159	42	[25]	710
PHBVV frac-A1	0.176	58	[25]	790
PHBVV frac-A2	0.106	40	[25]	850
PHBVV frac-A3	0.070	30	[25]	510
MCL-PHA	0.023	15.6	[34]	79
PHB	0.185	60	[25]	550

as nucleation sites. How the post-composite amorphous state has changed must also be further analyzed. Fig. 3 illustrates the absorbance light spectrum with composite microparticle of the PH4T16 composite over time. It was observed that wavenumber at 1043 cm^{-1}, the absorbance spectrum was greater than wavenumber at 1079 and 1110 cm^{-1}, while the absorbance wavenumber at 1210 cm^{-1} remained constant. According to the experiment, wavenumber at 1043 cm^{-1} was identified as the most prominent of PHB/TCP/HA crystallization, serving as an evident marker. The absorbance wavenumber at 1210 cm^{-1} was used as a reference point because it demonstrated a constant absorbance spectrum. In Fourier Transform Infrared Spectroscopy (FTIR) analysis, we use the absorbance at the wavenumber of 1210 cm^{-1} as a reference point because it demonstrates a constant absorbance spectrum. This constant absorbance allows us to have a stable point of comparison for observing changes in other parts of the spectrum. Having a constant reference point is crucial in FTIR analysis as it enables measurement and comparison of the intensity of light absorbed by different chemical bonds with precision. Substituting these values into Eq. 2 allowed for the calculation of instantaneous spectrum of absorbance, as shown in the Eq. 7.

$$AI_I = \frac{A_{1043}}{A_{1210}} \tag{7}$$

When AI_i is the instantaneous infrared absorption index, A_{1043} is the absorbance spectrum of PHB/HA/TCP at wave number 1043 cm^{-1}, and A_{1210} is the absorption intensity spectrum of PHB/HA/TCP at wavenumber 1210 cm^{-1}.

The infrared spectral absorbance curves (Fig. 4) depict the infrared spectral absorbance curves of six standard PHAs. Sample E comprised PHB utilizing glycerol as a substrate; Sample A represents the original PHBVV copolymer synthesized with glycerol and levulinic acid as substrates; Samples A1 to A3 are fractionated PHBVV copolymers, obtained through a meticulous fractional extraction process using chloroform; and MCL-PHA, produced with sodium octanoate as the substrate. The wavenumber 3436 cm^{-1} represented the hydroxyl group (-OH),

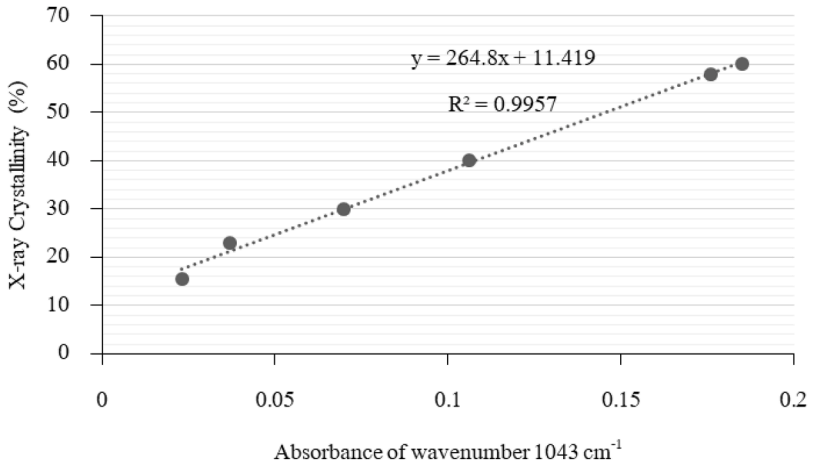

Fig. 5. Calibration curve of the relationship between absorbance from infrared spectra and X_c value of various types of PHA polymers.

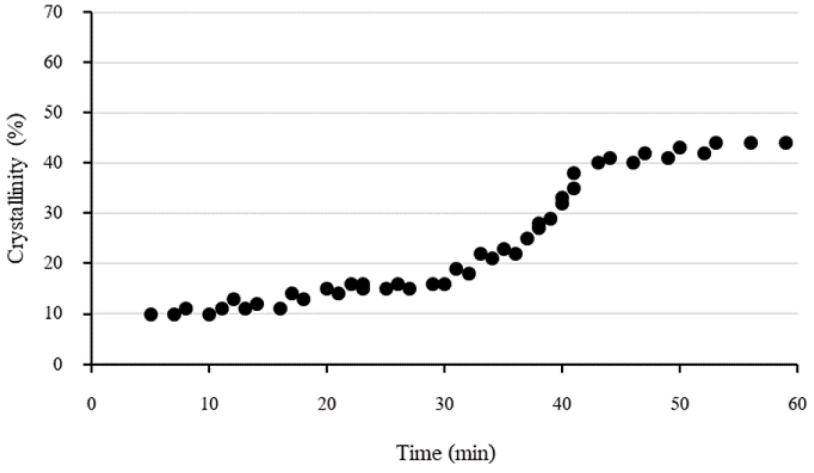

Fig. 6. Plot of degree of crystallinity with crystallization time of PHB/HA/TCP composite microparticle.

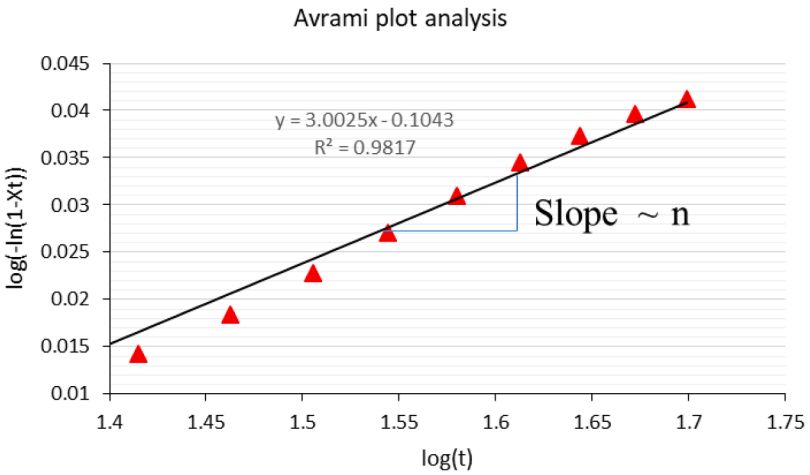

Fig. 7. Crystallization data fitted to the Avrami equation.

Table 5
The n, k values and the crystallization half-time of in-situ PHB/HA/TCP composite.

Sample	n [a]	k [b] (min^{-n})	$t_{1/2}$ [c] (min)	$1/t_{1/2}$ [d] (min)
PHB/HA/TCP	3.0025	2.20×10^{-5}	37.855	0.0264

[a] Avrami exponent.
[b] Growth rate parameter.
[c] Crystallization half time calculated from the Avrami equation.
[d] Overall crystallization rate.
Note: The results were obtained from a crystallization plot of the composite microparticles of PHB/HA/TCP under the condition of PHB:80, HA:4, TCP:16 (PH4T16).

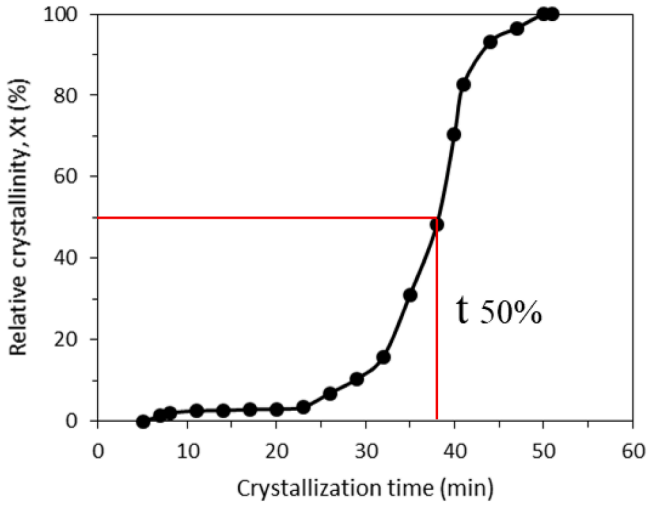

Fig. 8. The relative crystallinity curve with crystallization time.

wavenumber 2955, 2925, and 2855 cm^{-1} expressed a group of alkanes (CH_3-CH_2-CH_2- and -CH_2-CH_3), wavenumber 1737 cm^{-1} represented the carbonyl ester group (C=O), wavenumber 1300 cm^{-1} represented the group of Esters (C-O). Table 4 presents a comparison of the infrared absorbance spectroscopy of the six standard PHAs measured at wavenumber 1043 cm^{-1} compared to X_c values based on XRD treatment in the year 2013. It was found that the absorbance infrared spectra X_c has a direct correlation, if X_c is high, the infrared spectrum is also high. The calibration curve (Fig. 5) was plotted between the relationship of the absorbance spectra infrared at wavenumber 1043 cm^{-1} and X_c value of all 6 types of the PHAs. Linear equations can be derived and used as an equation and calibration curve for the crystallization calculation of PHB/HA/TCP composite microparticles.

From the calibration curve, the relation of the linear equation between the absorption of all six PHAs with the X_c value can be found using Eq. 8, whilst the instantaneous crystallization can be found via Eq. 9.

$$Y = 264.8(X) + 11.419 \quad (8)$$

$$R^2 = 0.9957$$

From the Eq. (7), when substituting AI_i into X,

$$Y = 264.8(AIi) + 11.419 \quad (9)$$

Where Y is instantaneous crystallization.

The percentage crystallinity of the PHB/HA/TCP composite microparticles over time is shown in Fig. 6. Data for 0–5 min are unavailable because HA and TCP must be added to the sample test during this period. However, from 5 to 30 min, the graph indicates that the composite microparticles of PHB/HA/TCP remain amorphous and only begin to crystallize after 30 min. The crystallinity of composite microparticles of PHB/HA/TCP increased to 44% at 60 min. Analyzing the crystallization curves and applying the Avrami equation, which is used to study the crystallization behavior of the polymer, allows the determination of the n and k values. These values indicate the morphology, the crystallization mechanism, and crystallization half-time of composite microparticles of PHB/HA/TCP, as illustrated in Fig. 7 and Table 5.

The crystallization curve of PHB/HA/TCP composite microparticles (Fig. 6) allowed us to determine the crystallization time using relative crystallinity curves. At 30 min, the crystallinity percentage reached 50 (Fig. 8). Comparing the crystallization half-time value with the time corresponding to 50% crystallization, we found the times to be approximately 37.85 min and 38 mins, respectively, validating the accuracy of the n and k values in the Avrami equation. These parameters, the Avrami constant (n) and crystallization rate constant (k), offer insights into crystallization behavior and sample morphology. Data from Table 5 suggest that sample PH4T16 exhibits sporadic crystallization behavior and has a disc-like morphology [35].

The Avrami exponent (n) and growth rate parameter (k) are of paramount importance in elucidating the crystallization behavior of PHB when incorporating bioceramics during spherulite formation. Previous studies have indicated that the crystallization of PHB varies depending on stimulating factors such as temperature changes or pH alterations [24]. Typically, spontaneously nucleated PHB exhibits a high Avrami exponent ($n > 1$), indicating extensive spherulite expansion. Meanwhile, the growth rate parameter of PHB under these conditions tends to be lower, suggesting fewer spherulite formations resulting in larger sizes due to the ample expansion space. Conversely, when PHB

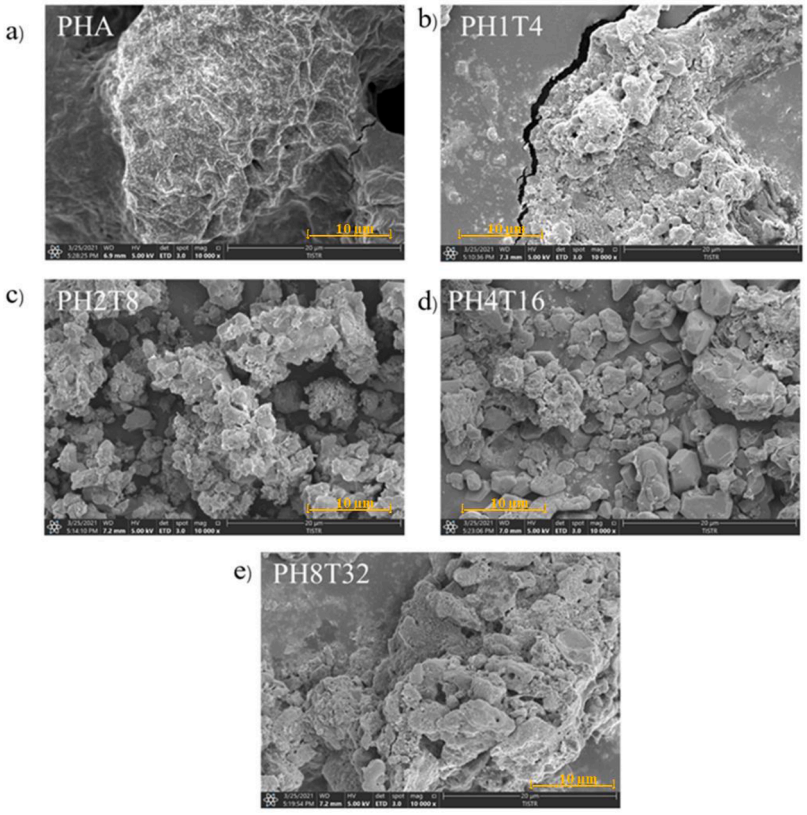

Fig. 9. SEM images (10000x) showing morphology of PHB/HA/TCP composite: a) PHB without compositing with HA and TCP, b) PH1T4 containing HA 1 and TCP 4 %, c) PH2T8 containing HA 2 and TCP 8, d) PH4T16 containing HA 4 and TCP 16 %, and e) PH8T32 containing HA 8 and TCP 32 %. Scale bars: 10 μm.

granules are stimulated, such as during the extraction process from bacteria, the Avrami exponent significantly decreases towards zero (n » 0) with an increase in pH due to the use of bases. This indicates reduced spherulite expansion. However, the growth rate parameter in such conditions tends to be higher than the stimulated PHB crystallization, suggesting a higher number of spherulites generated. Consequently, spherulites formed in PHB composites with hydroxyapatite (HA) and tricalcium phosphate (TCP) during spherulite formation resemble those spontaneously generated in pure PHB, as evidenced by the extensive spherulite expansion, albeit occurring only in select regions due to water elimination. This results in larger expansion areas, reflected in the higher Avrami exponent ($n > 0$) and lower growth rate parameter compared to stimulated PHB crystallization. Nevertheless, the Avrami exponent of PHB composites remains higher than that of general PHB, indicating fewer spherulite formations relative to the overall PHB crystallization. This may be attributed to the interference of HA and TCP within the PHB structure during spherulite formation.

This study investigated the crystallization behavior using the infrared light absorption spectra of the microparticle sample PHB/HA/TCP. This method monitored the crystallization formation from the amorphous state of the sample until it fully crystallized. The incorporation of HA and TCP into the origin of PHA resulted in a slower crystallization rate compared to the half-time crystallization of pure PHB. Generally, the crystallinity of PHB/HA/TCP (PH4T16) was about 44% after 60 min, whereas the crystallinity ratio of pure PHB was around 60%. This difference arises because HA and TCP do not act as nucleating agents to promote molecular aggregation, thus causing PHB to crystallize more slowly. From the previous study [36], PHB crystallization without incorporate HA and TCP took only 15–20 min for the crystallization to progress from 0 to 50%, compared to the crystallization half-time ($t_{1/2}$=38 min) in this PHB biocomposite study shown in Fig. 8. Due to the significant molecular size differences, PHB undergoes homogeneous nucleation, where PHB particles agglomerate and push HA and TCP to the outside, causing both bioceramics to be on the surface of the aggregated PHB molecules [37]. Incorporating HA and TCP into the structure of PHB during spherulite formation yields composite particles with a disc-like morphology, as approximated by the Avrami equation. This phenomenon indicates the entrapment of HA and TCP within the PHB structure, which differs from typical composites in applications such as bone regeneration for dentistry. Typically, these particles act as grafts for bone regeneration but are prone to rapid degradation upon exposure to bodily fluids if the composite is incomplete [38]. Therefore, the incorporation of these bioceramic composites into a PHB structure, which exhibits high hydrophobicity when spherulite formation is complete, may present itself as a viable solution to mitigate such issues. With a disc-like morphology and the fact that HA and TCP are composited on the surface of PHB, it may be beneficial for regeneration. The increased surface area might allow the bioceramics to contact tissue or promote efficient bone cell growth [39].

3.4. Morphology investigation using SEM

Fig. 9 shows an SEM image at a magnification of 10,000x, a) PHB without composite HA and TCP, b) PH1T4 with 1% HA and 4% TCP, c) PH2T8 with 2% HA and 8% TCP, d) PH4T16 with 4% HA and 16% TCP, e) PH8T32 with 8% HA and 32% TCP. The morphological comparison of the four PHB/HA/TCP composite microparticles to the control group with an SEM at magnification camera length 10000x revealed that HA and TCP were found on the surface of the PHB. If the content of HA and TCP exceeded 8% and 32%, respectively, sedimentation of HA and TCP was observed.

The morphology of the samples observed through the SEM revealed different surface characteristics between pure PHB and PHB/HA/TCP with particles of HA and TCP attached. An excessive or insufficient

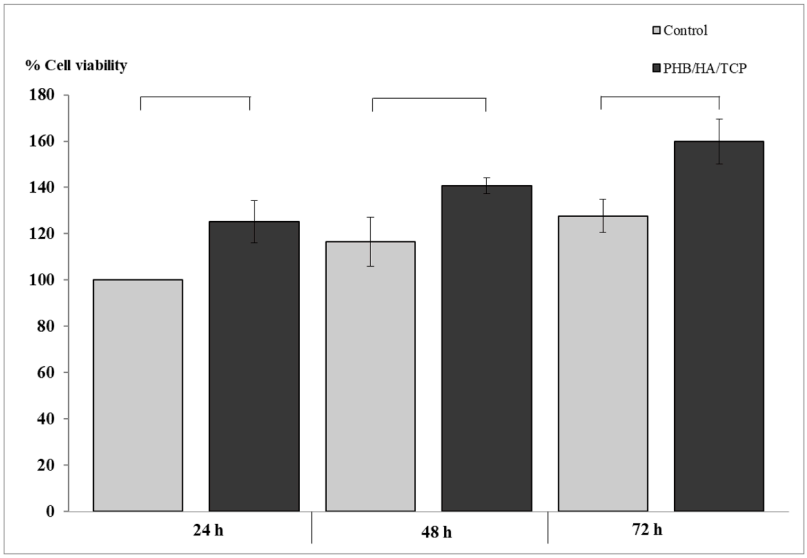

Fig. 10. Percentage of cell viability of control and PHB/HA/TCP groups at 24, 48, and 72 hours. The PHB/HA/TCP group showed a statistically significant difference compared to the control at all time points. The connected lines indicate statistically significant differences between the groups (p-value < 0.05).

amount of HA and TCP affects the stability of the sample, leading to particle agglomeration and a tendency for particle precipitates to form, as shown in Fig. 8e. This instability is further supported by zeta potential measurements, which indicate that only within a specific range of HA/TCP ratios does the composite achieve optimal dispersion, reducing agglomeration. The surface distribution of HA and TCP, influenced by their interactions with the PHB matrix, contributes to variations in surface roughness and porosity, which are key factors in material stability and function. However, the morphology of PHB/HA/TCP supports the previous hypothesis concerning the crystallization behavior of PHB, which pushes out HA and TCP to the outer surface during the homogeneous nucleation of PHB, causing the bioceramics to adhere to the surface of the PHB. The surface of the PHB composite particles, as observed from SEM images, differs from the PHB composites with bioceramics made by other methods, where HA and TCP are often embedded within the polymer matrix rather than being exposed on the surface, leading to less uniform distribution and potential phase separation. Our previous study composited PHB with HA using a filling method where PHB was filled into the HA scaffold, relying on mechanical forces from centrifugation [40]. The morphology of the surface materials composited in this manner shows a clear separation between the PHB matrix and HA, as observed from the surface in Figs. 9a and 9d. This is different from compositing by in-situ crystallization in this study, where HA and TCP particles are trapped onto the surface of PHB when crystallization is complete. In addition, the surface properties of the PHB microparticles might relate to the protein adsorption and release properties of hydroxyapatite, giving rise to in-situ crystallization [41].

3.5. Cell cytotoxicity of biocomposite microparticles

Fig. 10 illustrates the cell viability rate of the control and PHB/HA/TCP groups at 24, 48, and 72 hours. The PHB/HA/TCP group consists of 80% PHB, 4% HA, and 16% TCP. The results indicate that cell viability did not decrease over time in any of the tested groups. However, differences were observed in the rate of cell proliferation. Both groups containing HA and TCP showed a statistically significant difference in cell viability compared to the control group (p-value < 0.05). The cell viability test results indicate that the composite material does not exhibit cytotoxic effects on cells, which aligns with the inherent biocompatibility of its individual components before composite formation. Furthermore, these findings confirm that the compositing process does not leave behind any residual substances or by-products that could be harmful to cells. However, further studies may be required to evaluate its effectiveness in applications for dental bone regeneration.

Table 6
Environmental impact and energy use comparison between conventional and one-pot methods.

Impact category	Unit	Co-precipitation and sintering	One-pot recovery and in-situ crystallization
Global warming potential	kg CO_2eq	2.55	1.28
Non-renewable energy use	MJ deprived	34.9	17.5

3.6. Life cycle assessment of biocomposite microparticles

The life cycle assessment (LCA) of raw material acquisition and the compositing processes of HA and TCP for producing materials used in dental socket bone regeneration, as alloplastic bone grafts, was evaluated. This assessment compared the conventional method for producing market-available alloplastic bone graft HA/TCP (20:80) with the one-pot recovery and in-situ crystallization method, which incorporates PHB as a key component for compositing HA and TCP. The impact analysis focused on two primary categories: global warming potential (GWP) and non-renewable energy use (NREU). Both methods were analyzed under the same functional unit, defined as the amount of material required for implantation in a 15 $\times$ 10 mm^2 wound, corresponding to 0.15 g of material. Results from Table 6 and Fig. 11, which present the quantities and proportions of impacts from both methods, indicate that the one-pot method reduces GWP emissions by 50% compared to the conventional production method for market-available HA/TCP. Similarly, the NREU of the one-pot method showed a comparable reduction, indicating that this method consumes less energy during production. Although the input inventory of the one-pot method includes a broader list of required resources, the quantities used do not significantly influence the assessed environmental impacts. These results highlight the environmentally friendly potential of the products developed through this research.

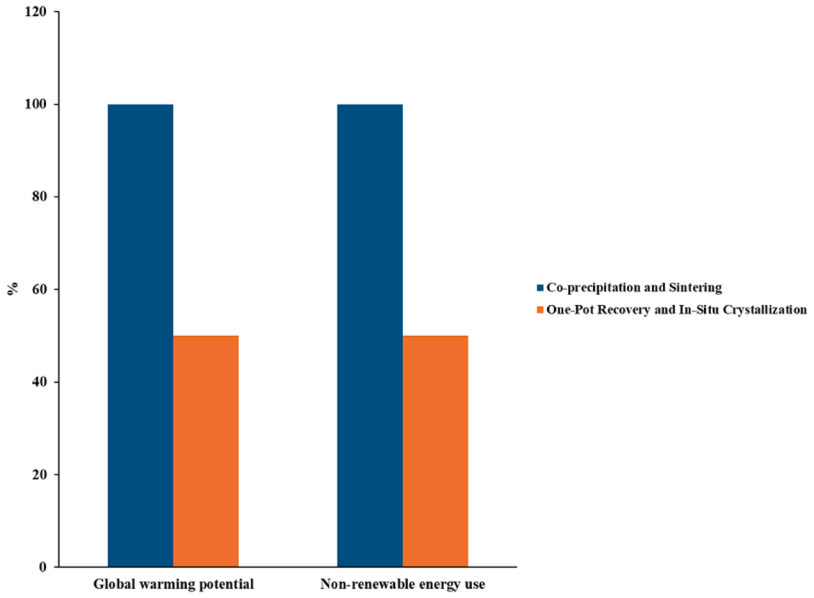

Fig. 11. Comparison of environmental impacts: global warming potential and non-renewable energy use for different compositing methods.

4. Conclusion

Production of PHB composites is an important step in improving their overall mechanical properties and in turn their usability in novel biomedical applications. The novel one-pot composite production strategy demonstrated in this study can minimize processing steps, complexities and costs compared to conventional multiple-step composite production. Valuable insights are provided into the facile one-pot strategy of incorporating HA and TCP into PHB to enhance the performance of both bioceramics, ensuring their homogeneity and optimal dispersion for more efficient dental bone restoration. By incorporating HA and TCP into the PHB polymer matrix during the extraction process, the measurements of the electrical zeta potential and particle size revealed that the microparticle PH4T16 composed of 80% PHB, 4% HA, and 16% TCP, which can be emerged as the most suitable composite material for practical applications. This is attributed to its excellent dispersion in the fluid and appropriate particle size, making it suitable for use in dental grafting materials. Furthermore, the crystallization behavior of the PH4T16 material mentioned was examined. The study of its crystallization patterns revealed sporadic occurrences and plate-like morphologies. The crystallization time for this material is somewhat slower than that of pure PHB, attributed to the incorporation of bioceramic particles of varying sizes into the PHB structure. This behavior results in PHB crystallizing independently without relying on a nucleating agent, causing the particles of HA and TCP to be segregated as the PHB begins to crystallize. SEM observations of morphology indicate that the particles of HA and TCP are located on the surface of the PHB with plate-like structures and well-dispersed in the liquid. This suggests that this composite material could be an efficient dental bone-filling material. Due to its high surface area and excellent fluid dispersion, it may contribute to more effective dental bone restoration compared to traditional bioceramics that lack stability when suspended in a liquid and might clump or settle, potentially reducing the efficiency of restoration. Moreover, the LCA of the novel composite method highlighted its environmental perspective compared to conventional market products. The results demonstrated a significant reduction in environmental impact rates and energy consumption, indicating that the new compositing process not only improves efficiency and stability during application but also exhibits environmental friendliness. Furthermore, compared to conventional compositing techniques, the one-pot in-situ crystallization approach reduces production time by integrating polymer recovery and composite formation into a single step. This eliminates the need for additional processing steps, reducing both material and energy costs. The ability to streamline the manufacturing process while maintaining efficiency makes this method highly suitable for scalable production. This positions the novel method as a promising candidate for large-scale production and competitive applications in the future. The novel one-pot synthesis method will also be highly beneficial for further development of biopolymer and biomaterial downstream processing, providing new materials for further development of novel biomedical applications.

Institutional review board statement

Not applicable.

Informed consent statement

Not applicable.

CRediT authorship contribution statement

Anuchan Panaksri: Writing – review & editing, Writing – original draft, Validation, Investigation, Formal analysis, Data curation. **Pasin Kuncharin:** Writing – original draft, Visualization, Methodology, Investigation. **Purin Neerawong:** Writing – original draft, Visualization, Methodology, Investigation. **Taranuch Panthong:** Visualization, Methodology, Investigation. **Thanadol Thanakornkriengkrai:** Visualization, Methodology, Investigation. **Sani Boonyagul:** Validation, Supervision, Formal analysis. **Woradej Pichaiaukrit:** Writing – original draft, Validation, Conceptualization. **Sutee Wangtueai:** Validation, Software, Resources, Project administration, Funding acquisition. **Nuankanya Sathirapongsasuti:** Validation, Supervision, Formal analysis. **Kittisak Jantanasakulwong:** Validation, Funding acquisition. **Pornchai Rachtanapun:** Validation, Funding acquisition. **Patnarin Worajittiphon:** Writing – original draft, Validation. **Phavit Wongsirichot:** Writing – review & editing, Writing – original draft, Validation. **Nuttapol Tanadchangsaeng:** Writing – review & editing, Writing – original draft, Validation, Supervision, Software, Resources, Project administration, Methodology, Investigation, Funding acquisition, Formal analysis, Conceptualization.

Declaration of competing interest

The authors declare that they have no known competing financial interests or personal relationships that could have appeared to influence the work reported in this paper.

Acknowledgments

This research was funded by National Research Council of Thailand (NRCT) (Flagship 2563; Project ID: 7147). The present study was partially supported by the Thailand Research Fund (TRF) Research Team Promotion Grant, RTA, Senior Research Scholar (N42A671052). This research work was also partially supported by Chiang Mai University. The authors appreciate financial support from Rangsit University.

Data availability

Data will be made available on request.

References

[1] S.P. Valappil, A.R. Boccaccini, C. Bucke, I. Roy, Polyhydroxyalkanoates in gram-positive bacteria: insights from the genera Bacillus and streptomyces, Antonie Van Leeuwenhoek 91 (2007) 1–17.
[2] M. Sharma, H.K. Dhingra, An overview of microbial derived polyhydroxybutyrate (PHB): production and characterization, Microb. Pol. Appl. Ecol. Perspect. (2021) 143–176.
[3] V. Fasiku, S. Owonubi, E. Mukwevho, B. Aderibigbe, E. Sadiku, O. Agboola, Y. Lemmer, W. Kupolati, K. Selatile, G. Makgatho, Polyhydroxyesters as scaffolds for tissue engineering, biosynthesis, Chemical Structures and Applications (2018) 167.
[4] R. de Sousa Victor, A. Marcelo da Cunha Santos, B. Viana de Sousa, G. de Araújo Neves, L. Navarro de Lima Santana, R. Rodrigues Menezes, A review on Chitosan's uses as biomaterial: tissue engineering, drug delivery systems and cancer treatment, Materials 13 (21) (2020) 4995.
[5] M. Degli Esposti, F. Chiellini, F. Bondioli, D. Morselli, P. Fabbri, Highly porous PHB-based bioactive scaffolds for bone tissue engineering by in situ synthesis of hydroxyapatite, Mater. Sci. Eng. C. 100 (2019) 286–296.
[6] J. Lim, M. You, J. Li, Z. Li, Emerging bone tissue engineering via polyhydroxyalkanoate (PHA)-based scaffolds, Mater. Sci. Eng. C. 79 (2017) 917–929.
[7] I. Ielo, G. Calabrese, G. De Luca, S. Conoci, Recent advances in hydroxyapatite-based biocomposites for bone tissue regeneration in orthopedics, Int. J. Mol. Sci. 23 (17) (2022) 9721.
[8] T. Monia, B.C. Ridha, Polymer-ceramic composites for bone challenging applications: materials and manufacturing processes, J. Thermoplast. Compos. Mater. (2023) 08927057231190066.
[9] N. Roveri, M. Iafisco, Evolving application of biomimetic nanostructured hydroxyapatite, Nanotechnol. Sci. Appl. (2010) 107–125.
[10] K.S. Almulhim, M.R. Syed, N. Alqahtani, M. Alamoudi, M. Khan, S.Z. Ahmed, A. S. Khan, Bioactive inorganic materials for dental applications: a narrative review, Mater 15 (19) (2022) 6864.
[11] V. Ingole, B. Sathe, A. Ghule, Bioactive ceramic composite material stability, characterization, Fund. Biomater. Ceramics (2018) 273–296.
[12] A.S. Salim, A. Al Hijazi, Evaluation of the effect of synthetic biomaterial (calcium phosphate ceramic) on healing of extracted tooth socket, J. Baghdad Coll. Dent. 22 (2010) 57–61.
[13] F. Ali, M. Radvar, E. Shayesteh, H.S. Mohammadipour, Clinical assessment of a synthetic biomaterial containing hydroxyapatite and beta tricalcium phosphate in socket preservation, Res. J. Pharm. Technol. 15 (11) (2022) 5126–5131.
[14] M. Sanda, M. Shiota, M. Fujii, K. Kon, T. Fujimori, S. Kasugai, Capability of new bone formation with a mixture of hydroxyapatite and beta-tricalcium phosphate granules, Clin. Oral Implants Res. 26 (12) (2015) 1369–1374.
[15] R. Zhao, R. Yang, P.R. Cooper, Z. Khurshid, A. Shavandi, J. Ratnayake, Bone grafts and substitutes in dentistry: A review of current trends and developments, Mol 26 (10) (2021) 3007.
[16] M. Piccinini, A. Rebaudi, V.M. Sglavo, F. Bucciotti, R. Pierfrancesco, A new HA/TTCP material for bone augmentation: an: In vivo: histological pilot study in primates sinus grafting, ImPlant Dent. 22 (1) (2013) 83–90.
[17] M.R.Zaheer Roohi, M. Kuddus, PHB (poly-β-hydroxybutyrate) and its enzymatic degradation, Polym. Adv. Technol. 29 (1) (2018) 30–40.
[18] M. Ambrosi, M. Raudino, I. Diañez, I. Martínez, Non-isothermal crystallization kinetics and morphology of poly (3-hydroxybutyrate)/pluronic blends, Eur. Polym. J. 120 (2019) 109189.
[19] A. Rezaei, M. Mohammadi, In vitro study of hydroxyapatite/polycaprolactone (HA/PCL) nanocomposite synthesized by an in situ sol–gel process, Mater. Sci. Eng. C. 33 (1) (2013) 390–396.
[20] K. Tanaka, S. Sugimoto, T. Tamiya, K. Yagi, S. Kobayashi, Improvement of strength and porosity of β-TCP/HA composited bone filling material synthesized by hydrothermal Hot-pressing, in: 2019 International Symposium on Micro-NanoMechatronics and Human Science (MHS), IEEE, 2019, pp. 1–6.
[21] N. Tanadchangsaeng, J. Yu, Microbial synthesis of polyhydroxybutyrate from glycerol: gluconeogenesis, molecular weight and material properties of biopolyester, Biotechnol. Bioeng. 109 (11) (2012) 2808–2818.
[22] J. Yu, L.X. Chen, Cost-effective recovery and purification of polyhydroxyalkanoates by selective dissolution of cell mass, Biotechnol. Prog. 22 (2) (2006) 547–553.
[23] H.C. Lim, M.L. Zhang, J.S. Lee, U.W. Jung, S.H. Choi, Effect of different hydroxyapatite:β-tricalcium phosphate ratios on the osteoconductivity of biphasic calcium phosphate in the rabbit sinus model, Int. J. Oral Maxillofac. Implants 30 (1) (2015) 65–72.
[24] M. Porter, J. Yu, Crystallization kinetics of poly (3-hydroxybutyrate) granules in different environmental conditions, J. Biomater. Nanobiotechnol. 2 (3) (2011) 301.
[25] N. Tanadchangsaeng, J. Yu, Miscibility of natural polyhydroxyalkanoate blend with controllable material properties, J. Appl. Polym. Sci. 129 (4) (2013) 2004–2016.
[26] S. Prakash, R. Mishra, R. Malviya, P.K. Sharma, Measurement techniques and pharmaceutical applications of zeta potential: a review, J. Chronother. Drug Del. 5 (2) (2014) 33–40.
[27] W. Kemper, R. Rosenau, Aggregate stability and size distribution, Methods of soil analysis: Part 1 Physical and mineralogical methods 5 (1986) 425–442.
[28] R. Greenwood, Review of the measurement of zeta potentials in concentrated aqueous suspensions using electroacoustics, Adv. Colloid. Interface Sci. 106 (1-3) (2003) 55–81.
[29] P. Makvandi, U. Josic, M. Delfi, F. Pinelli, V. Jahed, E. Kaya, M. Ashrafizadeh, A. Zarepour, F. Rossi, A. Zarrabi, Drug delivery (nano) platforms for oral and dental applications: tissue regeneration, infection control, and cancer management, Adv. Sci. 8 (8) (2021) 2004014.
[30] A. Padbury Jr, R. Eber, H.L. Wang, Interactions between the gingiva and the margin of restorations, J. Clin. Periodontol. 30 (5) (2003) 379–385.
[31] M.M. Nassar, K.I. Alzebdeh, T. Pervez, N. Al-Hinai, A. Munam, F. Al-Jahwari, I. Sider, Polymer powder and pellets comparative performances as bio-based composites, Iran, Polym. J. 30 (2021) 269–283.
[32] J. Li, J.A. Jansen, X.F. Walboomers, J.J. van den Beucken, Mechanical aspects of dental implants and osseointegration: A narrative review, J. Mech. Behav. Biomed. Mater. 103 (2020) 103574.
[33] S.V. Dorozhkin, Biocomposites and hybrid biomaterials based on calcium orthophosphates, Biomatter. 1 (1) (2011) 3–56.
[34] A. Panaksri, N. Tanadchangsaeng, Fractionation of medium-chain-length polyhydroxyalkanoate biosynthesized by pilot-scale production for improving material properties, Polym. Degrad. Stab. 213 (2023) 110368.
[35] V. Hinrichs, G. Kalinka, G. Hinrichsen, An Avrami-based model for the description of the secondary crystallization of polymers, J. Macromol. Sci. Phys. 35 (3-4) (1996) 295–302.
[36] L. Wang, X. Wang, W. Zhu, Z. Chen, J. Pan, K. Xu, Effect of nucleation agents on the crystallization of poly (3-hydroxybutyrate-co-4-hydroxybutyrate) (P3/4HB), J. Appl. Polym. Sci. 116 (2) (2010) 1116–1123.
[37] G. Ronca, *Heterogeneous Nucleation in Polymer Crystallization*, Brunel University School of Engineering and Design PhD Theses, 1985.
[38] M.N. Rahaman, D.E. Day, B.S. Bal, Q. Fu, S.B. Jung, L.F. Bonewald, A.P. Tomsia, Bioactive glass in tissue engineering, Acta Biomater. 7 (6) (2011) 2355–2373.
[39] G. Wang, J. Qiu, L. Zheng, N. Ren, J. Li, H. Liu, J. Miao, Sustained delivery of BMP-2 enhanced osteoblastic differentiation of BMSCs based on surface hydroxyapatite nanostructure in chitosan–HAp scaffold, J. Biomater. Sci. 25 (16) (2014) 1813–1827. Polymer Edition.
[40] M.M. Porter, S. Lee, N. Tanadchangsaeng, M.J. Jaremko, J. Yu, M. Meyers, J. McKittrick, Porous hydroxyapatite-polyhydroxybutyrate composites fabricated by a novel method via centrifugation, Mech. Biol. Syst. Mater. 5 (2013) 63–71. Proceedings of the 2012 Annual Conference on Experimental and Applied Mechanics, Springer.
[41] N. Jindapon, P. Klinmalai, U. Surayot, N. Tanadchangsaeng, W. Pichaiaukrit, Y. Phimolsiripol, C. Vichasilp, S. Wangtueai, Preparation, characterization, and biological properties of hydroxyapatite from Bigeye snapper (*Priancanthus tayenus*) bone, Int. J. Mol. Sci. 24 (3) (2023) 2776.